Mon. Not. R. Astron. Soc. **000**, 000–000 (0000) Printed 12 July 2002 (MN LATEX style file v1.4)

XMM-Newton EPIC observations of Her X-1*

Gavin Ramsay[1], Silvia Zane[1], Mario A. Jimenez-Garate[2,4], Jan-Willem den Herder[3], C. J. Hailey[4]

[1] *Mullard Space Science Lab, University College London, Holmbury St. Mary, Dorking, Surrey, RH5 6NT, UK*
[2] *MIT Center for Space Research, 77 Massachusetts Avenue, Cambridge, MA 02139, USA*
[3] *SRON, National Institute for Space Research, Sorbonnelaan 2, 3584 CA Utrecht, The Netherlands*
[4] *Columbia Astrophysics Laboratory, Columbia University, New York, NY 10027, USA*

Received:

ABSTRACT

We present spin-resolved X-ray data of the neutron star binary Her X-1 taken using the EPIC detectors on *XMM-Newton*. The data were taken at three distinct epochs through the 35 day precession period. The energy dependent light curves of this source vary significantly from epoch to epoch. It is known that the relative phasing of the soft ($\lesssim$1 keV) and hard ($\gtrsim$2 keV) X-rays varies. Here, we find that the phase shift between the soft and hard bands during the main-on state is considerably different from that observed in the past. Further, it continues to change significantly during the other two observations. This suggests that we are observing, for the first time, a *substantial and continuous variation in the tilt of the disk*, as it is expected if the accretion disk is precessing in the system. Analysis of the spin resolved data confirms that the equivalent width variation of the fluorescence Fe K line at $\sim$6.4 keV follows that of the soft X-ray emission in the main-on state, thus suggesting a common origin for Fe K line and thermal component. The Fe K line is considerably broader when the source is brightest.

Key words: accretion, accretion disks – X-rays: binaries – individual: Her X-1 – stars: neutron

1 INTRODUCTION

Her X-1 is an eclipsing binary system consisting of a neutron star and an A/F secondary star, HZ Her. Since its discovery, it has been observed extensively in many wavebands revealing a high degree of complexity in its behaviour. Her X-1 has a spin period of $\sim$ 1.24 s and a binary orbital period of 1.7 d (Tananbaum et al. 1972, Giacconi et al. 1973, Deeter, Boynton & Pravdo 1981, Oosterbroek et al. 2001). Eclipses are seen which recur on the timescale of the binary orbital period, indicating that the system has a high inclination. It also varies in X-rays on a period of 35 d, with a “main-on” state lasting $\sim$ 10 d and a secondary “short-on” state lasting $\sim$ 5 d. Between these states the source is fainter for $\sim$ 10 d.

The origin of the 35 d cycle is thought to be due to the precession of a tilted, warped accretion disk that periodically obscures X-rays from the central neutron star (see e.g. Gerend & Boynton 1976, Parmar et al. 1999, Ketsaris et al. 2000, Coburn et al. 2000). This idea is strengthened by the fact that optical emission from HZ Her persists at the same level throughout the main-on and low state, suggesting that the companion is still being irradiated by a strong X-ray source (Bahcall & Bahcall 1972, Bahcall 1978, Delgado et al. 1983).

The broadband X-ray spectrum of Her X-1 is also extremely complex. During the main-on state, the overall continuum is well described by a thermal blackbody component with temperature $kT_{bb} \sim 0.1$ keV, that dominates the spectrum at low energies (McCray et al. 1982, Oosterbroek et al. 1997), and a broken power-law plus an exponential cut off at higher energies. The galactic hydrogen column density in the direction of Her X-1 is low, $N_H \sim 10^{19} - 10^{20}$ atoms cm^{-2}.

In addition to these spectral features, at least three other components have been identified: i) a feature at $\sim$ 1 keV, often referred to as the ‘Fe L line’ (McCray et al. 1982, Oosterbroek et al. 1997; see also Mihara & Soong 1994, Oosterbroek et al. 2000 who reported a discrimination in two

* Based on observations obtained with XMM-Newton, an ESA science mission with instruments and contributions directly funded by ESA Member States and the USA (NASA).

narrow lines at 0.90 and 1.06 keV); ii) a broad Fe emission feature at ~ 6.4 keV (Pravdo et al. 1977, Choi et al. 1994, Oosterbroek et al. 1997, Coburn et al. 2000); iii) a cyclotron absorption feature at ~ 40 keV. The latter gives an inferred value of the magnetic field $\sim 3 \times 10^{12}$ G (see e.g. Dal Fiume et al. 1997).

An analysis of *Ginga*, *RXTE* and *BeppoSax* data (Mihara et al. 1991, Oosterbroek et al. 1997, Coburn et al. 2000, Oosterbroek et al. 2000) has shown that out with the main-on state the effects of a significant intervening absorption (with typical $N_H > 10^{21}$ atoms cm^{-2}) are clearly seen as a change in the spectral shape. However, a substantial flux remains below 0.5 keV that should be completely absorbed by such material unless the associated covering factor is partial (Oosterbroek et al. 2000). There are two possibilities which cannot be spectrally distinguished: a) the presence of two separate "scattering" and "absorbed" regions; b) an intrinsic partial covering of the emitting region, i.e. a situation in which the emission spectrum is the same in the low and main-on states, but a fraction of the emerging radiation is highly scattered and absorbed. Both cases are referred in the literature as "partial covering" models, and b) is what is expected, for instance, during occultation phases of the neutron star by the accretion disk.

Another manifestation of the 35 d precession cycle is the repeating, systematic evolution of the X-ray pulse profile over this cycle. Extensive coverage of these variations have been obtained using *Ginga* (Deeter et al. 1998). Simultaneous X-ray and UV observations have also been carried using *ASCA* and *HST* by Boroson et al. (1996), showing that the pulse shape becomes smooth and sinusoidal from the soft X-ray band into the UV (see also Leahy, Marshall, & Scott 2000). Past attempts to model the pulse changes in various energy bands relied on a combination of free neutron star precession and disk obscuration, as well as obscuration by flaps of matter at the magnetosphere or obscuration by the tilted disk (see Deeter et al. 1998, Scott, Leahy & Wilson 2000). However, most of these studies fail in explaining more than a few aspects of the complex pulse evolution. Recently, detailed interpretations have been presented by Deeter et al. (1998) and Scott et al. (2000). In particular, the model by Scott et al. (2000) is based on inner disk occultation of the X-ray beam from the neutron star. The latter, in turn, consists of two components: a pencil direct beam and a fan beam emission in the antipodal direction (see §7.1). This model refines the disk and pulsar beam geometry and qualitatively accounts for *both* the pulse phase *and* its evolution during the main-on and short-on high states.

In this paper we present the results of a series of three observations made using the EPIC cameras on board *XMM-Newton* at different Φ_{35} (see §2). We discuss the spin period of the neutron star in §3 and the pulse profile in different energy bands are reported in §4. In §5 we report the pulse-averaged broadband spectra, and in §6 we examine the pulse resolved spectra. We discuss our results in §7.

2 OBSERVATIONS

Her X-1 was observed using *XMM-Newton* on 3 separate occasions in 2001, the details of which are summarized in Table 1. The EPIC detectors (Turner et al. 2001; Strüder

Observation Date (orbit)	Effective Exposure (ksec)	EPIC PN Mean ct (ct/s)	Orbital Phase	35 d Phase
2001 Jan 26 (207)	10	398.4	0.19–0.25	0.17
2001 Mar 4 (226)	11	21.4	0.46–0.55	0.26
2001 Mar 17 (232)	11	54.3	0.51–0.59	0.60

Table 1. Summary of the *XMM-Newton* observations of Her X-1. For the orbital phasing we use the ephemeris of Still et al. (2001); for the 35 d phasing we define phase 0.0 at the main high state turn-on.

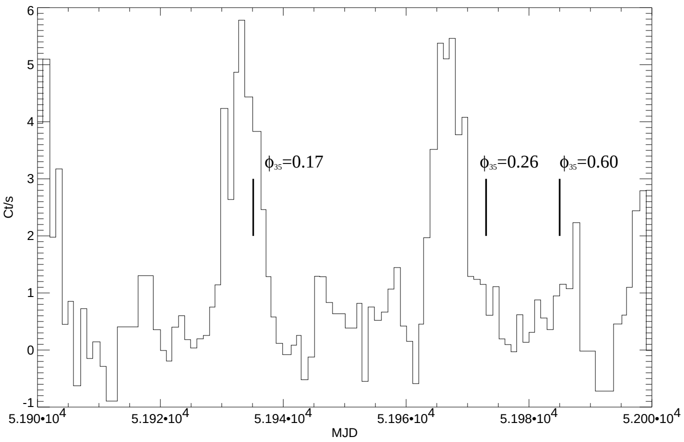

Figure 1. The *RXTE/ASM* (2-10) keV light curve of Her X-1: the thick lines indicate the *XMM-Newton* observations.

et al. 2001), were configured in timing mode (PN and MOS1) and full frame mode (MOS2) for all observations. The MOS2 data were heavily piled up and therefore are not used in the analysis. The medium filter was used in all observations. The *XMM-Newton* RGS observations are presented in a separate paper by Jimenez-Garate et al. (2002).

To determine how these observations relate to the 35 d precession period, we extracted the *RXTE ASM* (2-10) keV quick-look light curve (Figure 1). This shows that the first observation took place close to maximum X-ray brightness, while the third was close to the secondary maximum. The second observation took place after the end of the main-on state. The values of Φ_{35} corresponding to the three datasets are also reported in Table 1, where Φ_{35}=0.0 is the main-on state turn-on.

Data were processed using version 5.3.3 of the *XMM-Newton* Science Analysis System. Because the point spread function of the source covers most of the CCD which is read out, we are not able to reliably extract background light curves or spectra in the timing mode data. We did however examine the background light curves in the full frame data taken using the MOS2 detector. The background was relatively constant and low in the first (orbit 207) and last (orbit 232) observations. However, in the second observation (orbit 226) the particle background was high near the start and end of the observation: these times were excluded in the analysis. Since Her X-1 is much brighter than the background, we do not expect that the absence of background data will have a significant effect on our results.

We also had to correct two of the EPIC pn datasets for time jumps. In the case of orbit 207 a 1 sec time jump was found to take place at frame numbers 286698 and 646626. The cause of these time jumps is not known but are easily corrected for by subtracting 1 sec from the frame times for events occurring after these frame numbers. We also had to correct orbit 232 at frame number 514275 where `FTCOARSE` was incremented by 1 sec when it should not have done.

In this paper, in the interest of brevity, we report only the results derived using the EPIC pn data. This was because this data had a higher signal to noise than the EPIC MOS data. However, the results derived from the MOS data are consistent with those derived from the EPIC pn data.

This paper refines the work of Ramsay et al (2002) who present a prelimenary report of these *XMM-Newton* observations. In particular, the data reported by Ramsay et al were folded on different periods to the values reported below. This is because the routine used to correct events to the solar system barycenter (`barycen v1.9`) was incorrect. The spin folded light curves for Φ_{35}=0.26 and 0.60 reported by Ramsay et al (2002) are very similar to our present findings. In the case of the Φ_{35}=0.17 data, the general shape of the light curves are similar, but the details differ.

3 THE SPIN PERIOD

The spin period of Her X-1 has been found to vary from ∼1.23772 s to 1.23782 s, with alternating phases of spin-up and spin-down (Parmar et al. 1999, Oosterbroek et al. 2001). Furthermore, it can vary significantly on relatively short timescales. Before determining the spin period from our data, we first performed a barycentric correction (using `barycen v1.13.2`) and also a correction for the motion around the binary center of mass (using the ephemeris of Still et al. 2001) on each event photon (this was after the correction for the 1 sec time jumps reported above). We then determined the period, analyzing the data from each epoch separately using a Discrete Fourier Transform (Deeming 1975, Kurtz 1985). The best fit periods determined from the EPIC MOS and pn detectors are reported in Table 2.

The spin period at each epoch is consistent between the two EPIC detectors. Further the spin period taken from the first epoch (2001 Jan 26) is continuing to slow down after its long anomalous slow state: Oosterbroek et al (2001) determined a spin period of 1.2377697(3) in Oct 2000 using *BeppoSAX* data. Her X-1 was observed on 2001 Jan 25 using *Chandra*. The spin period was found to be 1.237786 sec (Burwitz, priv. comm). This spin period is marginally slower compared to our observation of Jan 26. Since the *Chandra* observation was configured in Grating mode and the frame time is slower than the EPIC timing mode, the *XMM-Newton* spin period is likely to be more accurate. There is a slight decrease in the spin period recorded in the two following epochs (2001 March).

4 SPIN RESOLVED LIGHT CURVES

We have extracted the light curves in various energy bands, at each of the three epochs. We then performed a least squares sinusoid fit to the light curves, using the best fit period appropriate to the epoch as previously found. The pulsed fraction, defined here as the modulation amplitude in the various energy bands divided by the mean count rate in that band, is shown in Table 3. We also folded and binned the same light curves, which are shown in Figure 2.

Observation	EPIC MOS (s)	EPIC pn
2001 Jan 26	1.2377727(7)	1.237774(5)
2001 Mar 4	1.23779(2)	1.237753(6)
2001 Mar 17	1.2377594^{+13}_{-5}	1.237751(3)

Table 2. The best fit periods determined from the EPIC MOS and pn light curves using a Discrete Fourier Transform. The number in parenthesis is the error on the last digit.

As we can see from Table 3, the relative modulation amplitude is strongest at $\Phi_{35} = 0.17$ (i.e. close to the main-on state). At this epoch, the value of the pulsed fraction is similar in all energy bands with the exception of the (0.8-1.2) keV range in which it is significantly lower. At $\Phi_{35} = 0.26$, the relative modulation amplitude is strongly reduced at all energies, but increases towards higher energies. At $\Phi_{35} = 0.60$, the relative modulation amplitude is again similar at energies above 2 keV and is a factor $\sim 2-3$ lower compared to that found in $\Phi_{35} = 0.17$.

The folded light curves corresponding to the different epochs are dramatically different (Figure 2). The softest X-ray emission (0.3-0.7keV) always shows a smooth, almost sinusoidal shape that is most prominent at $\Phi_{35} = 0.17$. At this epoch, the hard emission shows a prominent double peaked maximum, with the 'trailing' peak (peak 'B' in Figure 2) being less intense especially at harder energies. The phasing of those peaks corresponds to the minimum in the (0.3-0.7 keV) band. The (0.8-1.2 keV) light curve shows both the double peak seen at higher energies and also the broad maximum seen at lower energies. The (0.8-1.2) keV band shows a superposition of both the soft X-ray component and also the hard X-ray component.

In contrast, in the low-state ($\Phi_{35} = 0.26$) epoch the soft and hard X-ray light curves are very similar in shape and are roughly in phase.

Close to the short-on state ($\Phi_{35} = 0.60$), the maximum of the hard X-ray light curve corresponds to the minimum in the soft X-ray light curve. Further, at higher energies a secondary peak becomes more prominent (peak 'E' in Figure 2).

We also show the light curves in the energy range (6.2-6.6) keV. This energy range includes the emission from the Iron Kα emission line. In the main-on and also the low state, the folded light curve in this energy band is very similar to that of the (7-12) keV folded light curve. In the short-on state the general shape is very similar, although shortly after the descent from spin maximum there is a rise in flux compared to the minimum seen at higher energies. It is difficult to isolate the line emission from the continuum emission using these kind of light curves. We examine this further in §6, where we present the pulse resolved spectra.

Comparing the relative phasing of the soft and hard band we find that a turnover is evident after ~ 2 keV, in the main-on and short-on states. To determine the shift in phase between the hard and soft emission at each epoch, we have cross correlated the (0.3–0.7) keV and the (2–4) keV light curves for the two states $\Phi_{35} = 0.17$ and $\Phi_{35} = 0.60$.

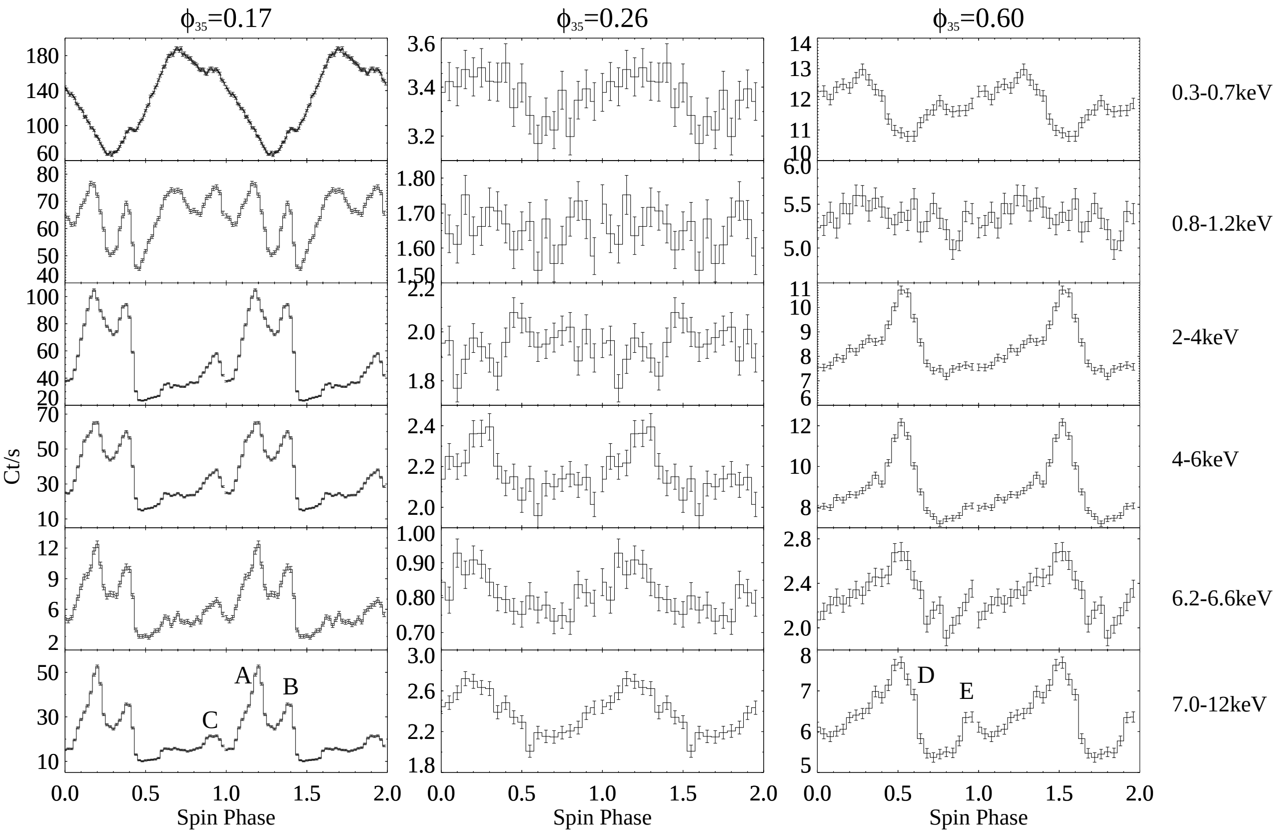

Figure 2. The spin profiles for various energy bands for the three epochs. Because of the uncertainty in the spin period in each epoch, the spin phases are not on the same absolute scale. The captions in the 7–12 keV band panels are refered to in the text.

Φ_{35}	0.3–0.7 keV	0.8–1.2 keV	2–4 keV	4–6 keV	6.15–6.7 keV	7.0–12.0 keV
0.17	0.399±0.004	0.097±0.003	0.400±0.004	0.292±0.004	0.341±0.012	0.235±0.004
0.26	0.029±0.005	0.022±0.010	0.027±0.010	0.049±0.009	0.071±0.013	0.111±0.009
0.60	0.059±0.007	0.024±0.008	0.136±0.042	0.164±0.006	0.098±0.009	0.110±0.006

Table 3. The pulsed fraction (modulation amplitude/mean count rate) over various spectral ranges for the 3 epochs.

For the fainter state ($\Phi_{35} = 0.26$) we determined the cross correlation between the (0.3–0.7) keV and (7–12) keV light curve, since the modulation in the latter band was higher than in the (2–4) keV band. We show the cross correlation in Figure 3.

Considering the main-on state first, we find that the most prominent cross correlation peak shows the soft and the hard light curves are strongly anti-correlated, with only a small phase lag ($\sim 330°$). We also find a strong positive peak at $\sim 150°$, which corresponds to the separation between the soft X-ray peak and the general peak in hard X-rays. The faint state shows a negative correlation at $\sim 180°$ and a positive correlation at small phase lag ($\sim 350°$), with the positive correlation having a higher coefficient. Again, the positive peak corresponds to the separation between maxima in the soft and hard lightcurves – they are basically in phase. During the short-on state, we find the highest, positive correlation near $\sim 90°$, which is due to the shift between the maximum in the soft and hard X-rays. It is evident that the relative phase shift between the soft and hard X-ray light curves varies as a function of the 35 d precession period. We discuss this further in §7.

5 THE PULSE AVERAGED X-RAY SPECTRA

As recommended by the *XMM-Newton* Science Operation Center, we ignore energies less than 0.5 keV in our spectral fits. The energy response file we use (epn_ti40_sdY9_medium.rsp), assumes only single and double pixel events, therefore we extracted only these events to construct the EPIC pn spectra. We extracted pulse averaged spectra at each epoch. We show the pulse averaged spectra taken at the three Φ_{35} in Figure 4. The immediate points to note are the apparent hardening of the spectra at lower intensity and the Fe K fluorescent line near 6.4 keV, that appears to become more prominent as the intensity weakens.

To model these spectra, we used an absorbed power law together with a blackbody and a Gaussian near 6.4 keV to

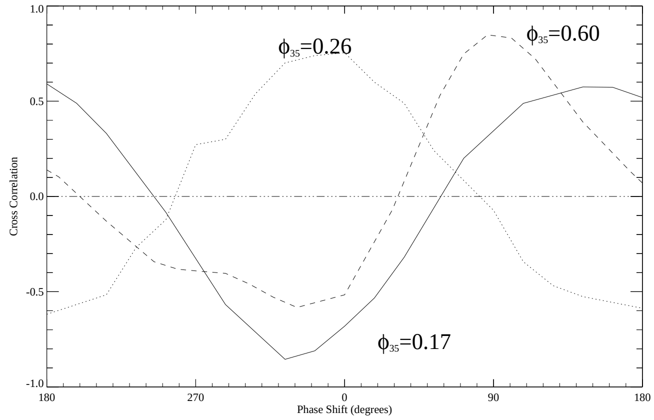

Figure 3. The cross correlations for the soft and hard energy resolved light curves at the 3 epochs.

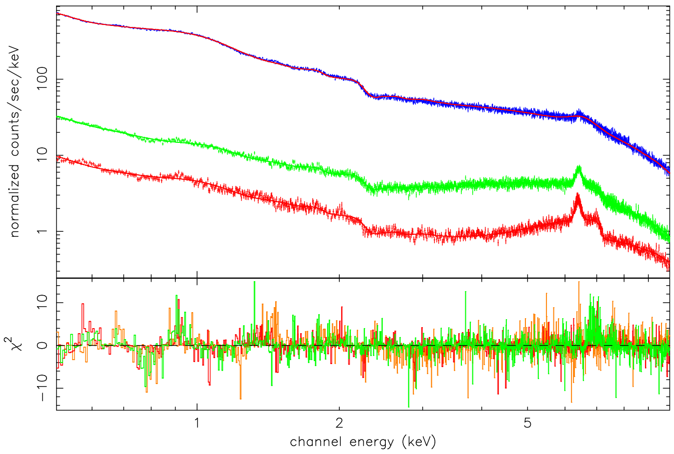

Figure 4. The EPIC pn spectra of Her X-1. From the top to the bottom: the spectra taken on Jan 26 (Φ=0.17), March 17 (Φ=0.26) and March 4 (Φ=0.60).

account for the fluorescence line. For the absorption model, we included a column of neutral Hydrogen fixed at the low value of 5×10^{19} cm^{-2}, which accounted for the interstellar absorption towards Her X-1. If a good fit was still not achieved we added additional partial covering models of neutral Hydrogen. We also included an additional Gaussian line at ~1 keV which was used to model the excess of emission at these energies found in the RGS spectra of the main-on state (Jimenez-Garate et al. 2002).

We show the spectral fits to the data in Table 4, where we also report the total observed flux in the (0.3-10) keV band, as well as the bolometric, unabsorbed blackbody flux and the unabsorbed power law flux. The fits to all three integrated spectra are reasonably good (χ^2_ν< 1.4).

We find that the absorption is highest at Φ_{35}=0.26, (when the source was at lowest intensity), and lowest at Φ_{35}=0.17 (when the source was at highest intensity). We also find that we need to include a blackbody component whose temperature is ~0.10 keV at each epoch. The fluorescence line at ~ 6.4 keV probably originates from irradiation of cold material (see §6 and §7.3). We find that its flux is greatest at Φ_{35}=0.17, when the line energy is higher compared to the other epochs. In addition, the line broadening changes significantly during the 35 d cycle: the full width half maximum (FWHM) increases by a factor ~4 when the source is brighter. The equivalent width is significant higher in the low state compared to the main-on or short-on state. We also searched for a second line at higher energies (features at 6.4 keV and 6.7 keV have been resolved with ASCA, Endo et al. 2000), but there was no evidence for a second emission feature. We discuss the spin variation in the Fe line profile in the next section.

	Φ_{35}=0.17	Φ_{35}=0.26	Φ_{35}=0.60
χ^2_ν	1.29 (1205)	1.09 (547)	1.17 (1195)
α	0.85	fixed	fixed
PL Norm	0.148	fixed	fixed
N_H, cvf		52^{+2}_{-3}, 0.82±0.01	12.6±0.5, 0.62±0.01
N_H, cvf		1000−50, 0.89±0.01	1500_{-1000}, 0.85±0.01

Table 5. The best fits to the EPIC pn spectra assuming a constant (power law) emission model based on the data obtained at Φ_{35}=0.17. We fit data in the energy bands (2.0-6.1) keV and (7-10) keV. The power law (PL) normalisation is in photons cm^{-2} s^{-1} keV^{-1} (at 1 keV), N_H is in units of 10^{22} atoms cm^{-2}, and "cvf" is the covering factor. When we allow the slope and normalisation of the power law to vary the goodness of fit is not significantly different.

The ratio of the unabsorbed, bolometric blackbody luminosity to the unabsorbed power law luminosity in the 0.01-100 keV range is ~1–2 per cent in all three epochs. This is significantly lower than that found by Endo et al (2000) using *ASCA* data (who found a ratio of 0.11)

In order to determine if the same (power law) model for the hard emission satisfactorily fits (apart from a local absorber) the spectra taken at the different epochs, we first re-computed the best-fit parameters of the power law for the Φ_{35}=0.17 spectrum. We ignored energies less than 2keV (where the blackbody component become visible and absorption becomes increasingly important) and energies between (6.1-7.0) keV (where the 6.4 keV fluorescence line is prominent). Keeping this model fixed, we then fitted the spectra taken at Φ_{35}=0.26 and Φ_{35}=0.60, by allowing the absorption to vary (adding a partial covering model if appropriate). We show the goodness of fits in Table 5. We find that a single power law emission model is consistent for all three epochs and the variation in the X-ray spectra is due to a variation in the amount of absorption. In a second step, we allowed the power law parameters to vary: the goodness of fit was not significantly different.

6 PULSE-RESOLVED SPECTROSCOPY

In order to investigate how the profile of the Fe line at 6.4 keV varies over the ~1.24 s spin period, we extracted spin resolved spectra from the EPIC data. We ignore energies below 5 keV and above 8 keV, and we used a Gaussian plus power law model to fit the spectra. We fix the absorption at the value found from the pulse averaged spectra (cf §5). We also fitted an absorbed power law over the range (2.0-6.1) keV and (7-10) keV – again we fix the absorption. The results are shown in Figure 5, together with the soft

	ϕ_{35}=0.17	ϕ_{35}=0.26	ϕ_{35}=0.60
N_H (atoms cm^{-2}), cvf		$56.1^{+0.7}_{-0.7} \times 10^{22}$, 0.79±0.01	$22.0\pm0.5 \times 10^{22}$, 0.54±0.05
N_H (atoms cm^{-2}), cvf		$10.3^{+1.2}_{-0.7} \times 10^{22}$, 0.29±0.01	$5.7\pm0.1 \times 10^{22}$, 0.51±0.01
kT_{bb} (eV)	101±1	104^{+1}_{-2}	102±1
α	0.90±0.01	$0.87^{+0.05}_{-0.01}$	1.05±0.01
Fe K line center (keV)	$6.540^{+0.018}_{-0.017}$	$6.385^{+0.005}_{-0.007}$	6.417±0.005
FWHM (keV)	$0.28^{+0.03}_{-0.02}$	$0.059^{+0.006}_{-0.013}$	$0.069^{+0.008}_{-0.007}$
line normalisation	$4.9\pm0.4 \times 10^{-3}$	$7.0^{+0.3}_{-0.5} \times 10^{-4}$	$9.8^{+0.24}_{-0.3} \times 10^{-4}$
EW (eV)	164^{+13}_{-12}	208^{+8}_{-14}	179^{+10}_{-6}
Observed flux (0.3-10) keV	$3.38\pm0.01 \times 10^{-9}$	$1.10\pm0.03 \times 10^{-10}$	$3.35\pm0.01 \times 10^{-10}$
Blackbody observed flux (0.3-10) keV	$3.53\pm0.05 \times 10^{-10}$	$4.21\pm0.13 \times 10^{-12}$	$1.32\pm0.15 \times 10^{-11}$
Blackbody bolometric flux	$6.62\pm0.05 \times 10^{-10}$	$5.18\pm0.15 \times 10^{-11}$	$1.06\pm0.02 \times 10^{-10}$
Power law observed flux (0.3-10) keV	$2.82\pm0.05 \times 10^{-9}$	$1.02\pm0.11 \times 10^{-10}$	$3.12\pm0.02 \times 10^{-10}$
Power law unabsorbed flux (0.01–99) keV	$3.65\pm0.05 \times 10^{-8}$	$4.3\pm0.1 \times 10^{-9}$	$4.95\pm0.02 \times 10^{-9}$
χ^2_ν	1.35 (1685)	1.18 (943)	1.31 (1673)

Table 4. The best fit parameters to the EPIC pn pulse averaged spectra. All errors are quoted at the 90 percent level. A constant column density of 5×10^{19} atoms cm^{-2} was also included, to account for the interstellar absorption. The units for the fluxes are erg cm^{-2} s^{-1}; the line normalisation is in photons cm^{-2} s^{-1}; FWHM is the full width half maximum; EW is the equivalent width and "cvf" is the covering factor.

and hard light curves. (In the case of the Φ_{35}=0.26 data we also fix the slope of the power law at the best fit value determined from the pulse averaged spectra since these data had the lowest signal to noise).

At Φ_{35}=0.26 and 0.60 there is no significant variation in the line parameters. At Φ_{35}=0.17, where the data have the highest signal to noise ratio, there is clear evidence that the equivalent width varies over the spin period with the minimum occurring at the phase corresponding to the maximum in hard X-ray intensity. Conversely the equivalent width is at maximum at the same spin phase that the soft X-ray is at its broad maximum intensity. This further supports the view that the 6.4 keV fluorescence Fe line and the black body component originate from a common region. There is some evidence that the line width varies over the spin phase with a maximum occurring immediately before the rise to hard X-ray maximum.

As expected the normalisation of the power law component follows the hard X-ray intensity modulation in the main-on and secondary-on state. In the case of the low state there is no evidence for a significant variation.

7 DISCUSSION

The results reported in this paper show for the first time that there is a continuous variation in the relative phase offset between the soft and hard X-ray components. We also find that normalisation and equivalent width of the fluorescence Fe line at 6.4 keV are modulated in phase with the soft X-ray component. Further, we find that for energies above ∼2 keV the three spectra corresponding to three different Φ_{35} are consistent with a single emission model and an absorption component which is lowest at Φ_{35}=0.17, and highest at Φ_{35}=0.26. Both the inferred values of N_H and covering factor for the intervening matter are consistent with Coburn et al. (2000), with the former considerably higher than that reported by Oosterbroek et al. (2000). We also require more than one partial covering component, and both these facts hint towards a fairly complex substructure of the thermal emission. On the other hand, the nature of the soft X-ray emission is not well understood and deserves a further, more detailed investigation. We now proceed by discussing the physical implications of our results.

7.1 The energy resolved light curves

The pulse profile of Her X-1 is known to evolve through the main-on state; those reported here closely resemble that observed using *Ginga* (Deeter et al. 1998). The EPIC observations taken at Φ_{35} = 0.17 and Φ_{35} = 0.26 can be qualitatively compared to Figure 6 of Deeter et al. (1998; main state D), while those taken at Φ_{35} = 0.60 are similar to their Figure 7 (short state C). Many of those features are naturally explained within the scenario proposed by Scott et al. (2000). This model was originally developed to explain *Ginga* and *RXTE* observations, and it is based on the obscuration of a multi-component X-ray beam by a counter-precessing, tilted, twisted disk. For simplicity, the X-ray beam is assumed to be decoupled from the disk and is axi-symmetric; the observer's line of sight must be close to the binary plane (to explain two maxima per 35 d cycle). One of the main features of this model is that it ascribes the variations observed in the pulse profile over the 35 d cycle to occultation from the *inner* part of the disk, whereas most of the previous investigations have assumed an occultation from the *outer* boundary (but see also Petterson, Rothschild & Gruber, 1991, who argued that vertical "flaps" which form near the magneto-spheric radius are partly responsible for the 35 d phase behaviour). Inner disk phenomena, in fact, are more plausible in explaining the peaks evolution of the spin profile, as well the differences in the pulse-shape of main-on and short-on. Such differences require that the size of the dominant pulse-emitting region is roughly the scale-height of the inner disk, so that the two high states are caused by progressive occultation of an *extended* source.

The complex pattern of peaks observed in Her X-1 can

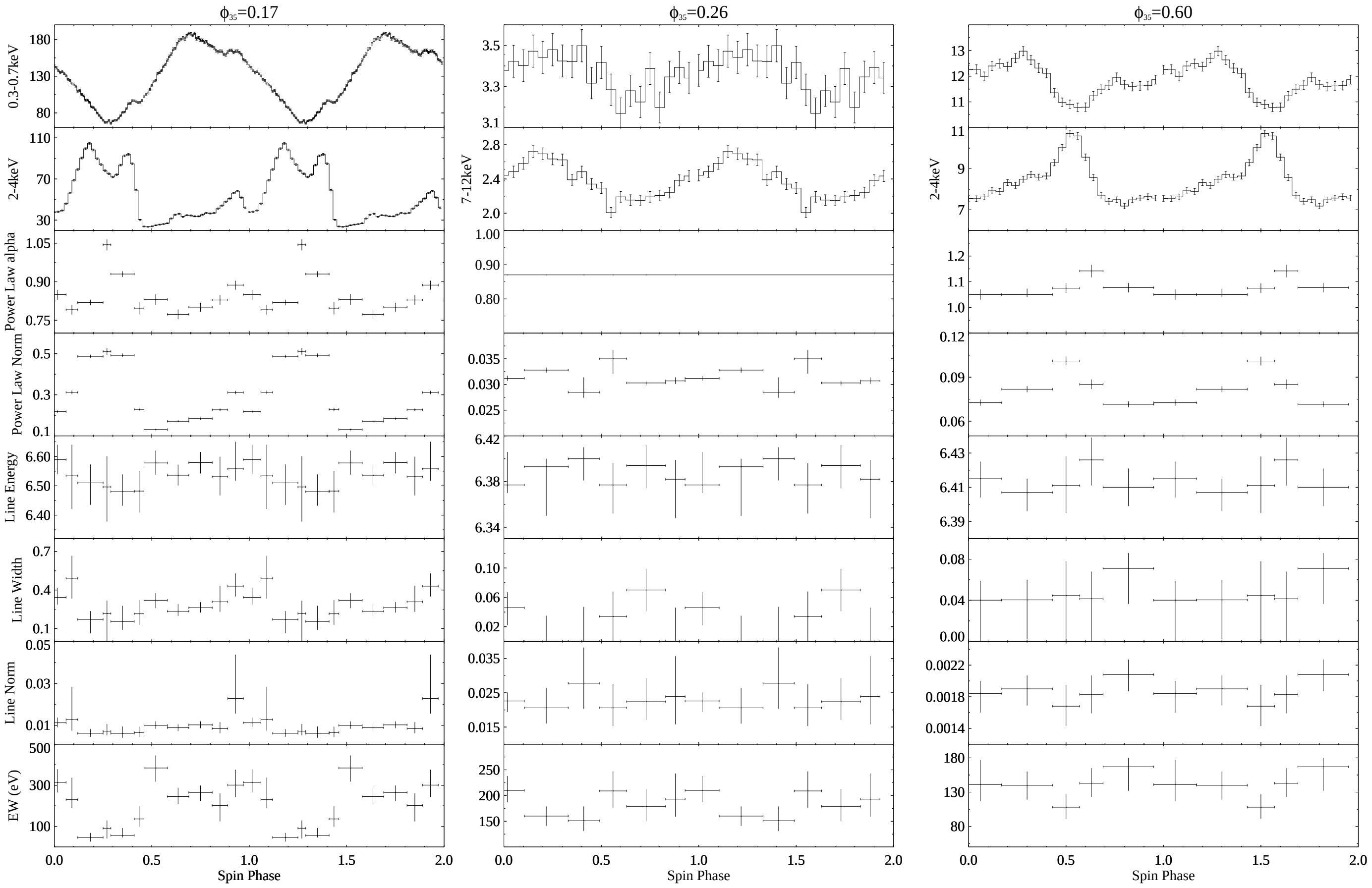

Figure 5. The variation of the Fe line parameters as a function of spin phase, for the three different epochs Φ_{35}. We also show the normalization of the power law component and the intensity curves in the soft (0.3-0.7 keV) and hard energy band. The latter is taken to be (2-4) keV for Φ_{35}=0.17, Φ_{35}=0.60 and (7-12) keV for Φ_{35}=0.26. The line width is the FWHM. The slope of the power law was fixed at Φ_{35}=0.26.

be explained in terms of successive occultations of a beam consisting of a direct pencil beam (that originates close to the poles at the surface of the neutron star) plus a reversed fan beam that is focused in the antipodal direction. These two components are superimposed on three other constant flux components: two due to magneto-spheric emission and one due to low-state coronal emission. In the "reversed fan beam" geometry, the fan beam component originates at the same distance above the neutron star surface and has an opening angle $> 90°$. A similar configuration has been predicted theoretically by Brainerd & Meszaros (1991), who studied the backscattering of the magnetic polar cap radiation by the incoming accretion flow and its subsequent gravitational focusing around the neutron star. The accretion column is predicted to be optically thin to Thomson scattering, while the fan beam photons are produced by cyclotron resonance scattering.

The overall situation is summarized in the bottom panel of Figure 8 in Scott et al. (2000), while their Figures 10a-10b illustrate the evolution of the pulse profiles predicted during the main-on and short-on respectively. A number of the features observed in our *XMM-Newton* data are qualitatively reproduced. At $\Phi_{35} = 0.17$, the hard emission shows two main peaks ('A' and 'B' in Figure 2), and a third, lower peak ('C' in Figure 2). This situation is close to that modeled by Scott et al. (2000) at similar Φ_{35}, during the progressive occultation of leading and training peaks of the hard beam. At $\Phi_{35} \sim 0.27$, when the main components are occulted, we only observe the survival of a broad, underlying modulation that is attributed to the magneto-spheric emission. Since this component is emitted from a larger region at some distance from the neutron star, it is naturally expected to have a lower modulation as well as a broad maximum (Figure 2).

The pulse profile close to the short-on is also similar to that presented by Scott et al. (2000) at $\Phi_{35} \approx 0.58$ (see their Figure 10b). In the EPIC data, we can in fact recognize a main peak 'D' as well a less prominent peak 'E' (Figure 2). A cross-correlation between different *XMM-Newton* datasets does not allow a proper phase alignment between main-on and short-on peaks based on the extrapolation of the pulse timing ephemeris. However, because the peak 'E' is the hardest feature, spectral considerations suggest that this maximum is associated with the small hard peak and the feature 'D' with the soft peak discussed by Scott et al. (2000). If this is the case, 'E' is actually due to direct emission from the pencil beam, while 'D' is the radiation redirected into the fan beam from the antipodal accretion column.

7.2 The phase shift between the soft and hard light curves

Given the complexity of the source, pulse-phase spectroscopy is of paramount importance to separate the different spectral components observed in Her X-1. Using *Einstein* (McCray et al. 1982) and *BeppoSax* data (Oosterbroek et al. 1997, 2000) it has been shown that, during the main-on state, the maximum of the thermal component and the power law components are shifted by $\sim 250^\circ$ and that the maximum of the unresolved feature at ~ 1 keV is in phase with that of the blackbody component. The situation is less consistent as far as the 6.4 keV Fe K line is concerned: Choi et al. (1994) have shown that its intensity is modulated in phase with the soft emission, suggesting a common origin for the two Fe lines, while Oosterbroek et al. (2000) have found it correlated with the hard (power law) emission.

The shift in phase between hard and soft emission can be explained if the latter results from re-processing of hard X-rays in the inner part of the accretion disk. If a non-tilted disk intercepts (and re-processes) a substantial fraction of the hard beam from the neutron star, the expected phase difference between direct and reflected component is 180°. Therefore, the value of $\sim 250^\circ$ determined using *Einstein* and *BeppoSax* data has been associated with the disk having a tilt angle. If the tilt of the disk changes with phase along the 35 d cycle (as predicted by the precessing disk models, see Gerend & Boyndon 1976) the shift in phase should therefore vary with Φ_{35}. However, both Einstein and Sax data were obtained at the same Φ_{35}, i.e. during the main-on state ($\Phi_{35} = 0.1$ for *Einstein*; $\Phi_{35} = 0.07 - 0.15$ for *BeppoSax* in 1997 and $\Phi_{35} = 0.1 - 0.2$ for *BeppoSax* in 2000). Oosterbroek et al. (2000) also observed the source at $\Phi_{35} = 0.5$ and found that the pulse phase difference in the short-on and main-on state are consistent. This is not surprising, since symmetry considerations allow for the same behaviour at $\Phi_{35} = 0.0$ and 0.5. A tracking of the phase difference between the two components over the entire cycle was therefore required.

Here we have found that not only the phase shift derived from *XMM-Newton* main-on data is considerably different from previous observations made in the main-on, but it continues to change dramatically during the other two observations. This suggests that we are observing, for the first time, a *substantial and continuous variation in the tilt of the disk*, which is what we would expect from a system which had a precessing accretion disc. It should be noted that the interpretation of the phase shift observed at the short-on may be affected by a systematic error, depending on whether during the observation the soft peak ‘D’ is higher than the small hard peak ‘E’ or vice-versa (see §7.1).

7.3 The fluorescent line variation

To investigate in more detail the possible common origin of the soft component and the Fe line at 6.4 keV, we have derived the line parameters as a function of the spin phase, ϕ_{spin} (see §6 and Figure 5). At Φ_{35}=0.26 and 0.60, there is little evidence for a significant variation in the line parameters.

The observation made during the main-on ($\Phi_{35} = 0.17$) clearly shows that the soft flux below 0.7 keV and the equivalent width all exhibit a common minimum at $0.2 \lesssim \phi_{spin} \lesssim 0.4$, which, in turn, is shifted with respect to that of the hard emission. This supports the idea that the 6.4 keV Fe line originates from fluorescence from the relatively cold matter of the illuminated spot where the soft emission is reprocessed. In this case, the flux emitted in the line may provide a lower limit to the size of the spot because the observed line energy allows us to put an upper limit to the ionization degree and to the temperature of the emitting region, $T \lesssim 0.3$ keV (Kallman & McCray 1982). This is in principle appealing since it allows us to constrain the size of the illuminated spot in a way which is less subject to absorption (compared with the usual methods based on the value of the soft flux). However, assuming a spherical spot and a distance to the source of 6.6 kpc (Reynolds et al. 1997), the inferred lower limit for the radius is $R \gtrsim 0.5$ km, too low to add any significant constraints. For comparison, assuming the same distance for the source, the radius of the equivalent blackbody derived from the soft flux varies between ~ 140 km and 500 km.

We have also found evidence for a variation in the Fe line parameters over the 35 d period. The line flux and the line width is greatest at the main-on state. We also show that the line energy is significantly higher in the main-on state and lowest in the low state. In the main-on state, the energy of the Fe line (6.540keV) corresponds to Fe XX-XXI, while in the low state (6.385keV) it is from low ionisation species.

This suggests two possible explanations for both the line broadening and the centroid displacement: 1) an array of Fe K fluorescence lines exists for a variety of charge states of Fe (anything from Fe I-Fe XIII to Fe XXIII); 2) Comptonization from a hot corona with a significant optical depth for a narrower range of charge states centered around Fe XX. Similar line broadening have been observed in some Low Mass X-Ray binaries observed using *ASCA* (Asai et al. 2000).

The Fe line broadening may also be explained in terms of Keplerian motion, if the inner disk (or some inner region) comes into view during the main-on state. If this is the case, at $\Phi_{35} = 0.17$ the Keplerian velocity will be ~ 13000 km/sec. This, in turn, corresponds to a radial distance of $\sim 4 \times 10^8$ cm (for a neutron star of $1.4 M_\odot$), which is close to the magnetospheric radius for a magnetic field of $\sim 10^{12}$ G.

8 ACKNOWLEDGMENTS

We would like to thank both Tim Oosterbroek and Uwe Lamers for providing help in resolving the timing problems found in the EPIC pn data. This paper makes use of quick-look results provided by the ASM/RXTE team whom we thank. We are grateful to Mariano Mendez, Vadim Burwitz and Mark Cropper for useful discussions.

REFERENCES

Asai, K., Dotani, T., Nagase, F., & Mitsuda, K. 2000, ApJS, 131, 571

Bahcall, J.N., & Bahcall, N.A. 1972, ApJL, 178, L1

Bahcall, J.N. 1978, in Physics and Astrophysics of Neutron Stars and Black Holes, ed. R. Giacconi and R. Ruffini (North-Holland Publishing Company, Amsterdam), p.63

Boroson, B., Vrtilek, S. D., McCray, R., Kallman, T., & Nagase, F. 1996, ApJ, 473, 1079
Brainerd, J.J., & Meszaros, P. 1991, ApJ, 369, 179
Choi, C.S., Nagase, F., Makino, F., Dotani, T., Kitamoto, S., Takahama, S. 1994, ApJ, 437, 449
Coburn, W., Heindl, W. A., Wilms, J., Gruber, D. E., Staubert, R., Rothschild, R. E., Postnov, K. A., Shakura, N., Risse, P., Kreykenbohm, I., Pelling, M. R. 2000, ApJ, 543, 351
Dal Fiume, D., Orlandini, M., Cusumano, G., del Sordo, S., Feroci, M., Frontera, F., Oosterbroek, T., Palazzi, E., Parmar, A. N., Santangelo, A., & Segreto, A. 1997, Proceedings of the Fourth Compton Symposium, ed. Charles D. Dermer, Mark S. Strickman, and James D. Kurfess (Williamsburg, VA April 1997: AIP Conference Proceedings 410), p. 758.
Deeter, J.E., Boynton, P.E., & Pravdo, S.H. 1981, ApJ, 247, 1003
Deeter, J.E., Scott, D. M., Boynton, P. E., Miyamoto, S., Kitamoto, S., Takahama, S., Nagasem F. 1998, ApJ, 502, 802
Deeming, T. J. 1975, Ap&SS, 36, 137
Delgado, A.J., Schmidt, H.U., & Thomas, H.C. 1983, A&A, 127, L15
Endo, T., Nagase, F., & Mihara, T. 2000, PASJ, 52, 223
Gerend, D., & Boynton, P.E. 1976, ApJ, 209, 562
Giacconi, R., Gursky, H., Kellogg, E., Levinson, R., Schreier, E., Tananbaum, H. 1973, ApJ, 184, 227
Jimenez-Garate, M. A., Hailey, C. J., den Herder, J. W., Zane, S., Ramsay, G., 2002, in press, ApJ
Kallman, T. R., McCray, R. 1982, ApJS, 50, 263
Ketsaris, N.A., Kuster, M., Postnov, K.A., Prokhorov, M.E., Shakura, N.I., Staubert, R., & Wilms, J. 2000, Invited talk presented at workshop of Bogolyubov Theoretical Physics Laboratory of JINR (Dubna) "Hot topics in astrophysics", astro-ph/0010035
Kurtz, D. 1985, MNRAS, 213, 773
Leahy, D.A., Marshall, H., & Scott, D. M. 2000, ApJ, 542, 446
McCray, R.A., Shull, J. M., Boynton, P. E., Deeter, J. E., Holt, S. S., White, N. E. 1982, ApJ, 262, 301
Mihara, T., Ohashi, T., Makishima, K., Nagase, F., Kitamoto, S., Koyama, K. 1991, PASJ, 43, 501
Mihara, T., & Soong, Y. 1994, in: Makino F. (ed.) Proc. of New Horizon of X-ray Astronomy, Universal Academy, Tokyo, p.419
Oosterbroek, T. Parmar, A. N., Martin, D. D. E., Lammers, U. 1997, A&A, 327, 215
Oosterbroek, T., Parmar, A. N., Dal Fiume, D., Orlandini, M., Santangelo, A., Del Sordo, S., Segreto, A. 2000, A&A, 353, 575
Oosterbroek, T., Parmar, A. N., Orlandini, M., Segreto, A., Santangelo, A., Del Sordo, S., 2001, A&A, 375, 922
Parmar, A.N., Oosterbroek, T., Dal Fiume, D., Orlandini, M., Santangelo, A., Segreto, A., del Sordo, S. 1999, A&A, 350, L5
Petterson, J. A., Rothschild, R. E., & Gruber, D.E. 1991, ApJ, 378, 696
Pravdo, S.H., Becker, R. H., Boldt, E. A., Holt, S. S., Serlemitsos, P. J., Swank, J. H. 1977, ApJ, 215, L61
Ramsay, G., Zane, S., Jimenez-Garate, M. A., den Herder, J. W., Hailey, C. J., 2002, In '*New Visions of the X-ray universe in the XMM-Newton and Chandra Era*, ESA SP-488, ed Jansen, F.
Reynolds, A. P., Quaintrell, H. Still, M. D., Roche, P., Chakrabarty, D., Levine, S. E. 1997, MNRAS, 288, 43
Scott, D.M., Leahy, D.A., Wilson, R.B. 2000, ApJ, 539, 392
Still, M., O'Brien, K., Horne, K., Hudson, D., Boroson, B., Vrtilek, S. D., Quaintrell, H., Fiedler, H., 2001, ApJ, 553, 776
Strüder, L., et al. 2001, A&A, 365, L18
Tananbaum, H., Gursky, H., Kellogg, E. M., Levinson, R., Schreier, E., Giacconi, R. 1972, ApJ, 174, L143
Turner, M., et al. 2001, A&A, 365, L27